Enzyme Dynamics along the Reaction Coordinate: Critical Role of a Conserved Residue

Evgenii L. Kovrigin and J. Patrick Loria*

Yale University, Department of Chemistry, Post Office Box 208107, New Haven, Connecticut 06520

Received December 8, 2005; Revised Manuscript Received January 11, 2006

ABSTRACT: Conformational flexibility of the enzyme architecture is essential for biological function. These structural transitions often encompass significant portions of the enzyme molecule. Here, we present a detailed study of functionally relevant RNase A dynamics in the wild type and a D121A mutant form by NMR spin-relaxation techniques. In the wild-type enzyme, the dynamic properties are largely conserved in the apo, enzyme−substrate, and enzyme−product complexes. In comparison, mutation of aspartic acid 121 to alanine disrupts the timing of active-site dynamics, the product-release step, and global conformational changes, indicating that D121 plays a significant role in coordinating the dynamic events in RNase A. In addition, this mutation results in 90% loss of catalytic activity despite the absence of direct participation of D121 in the chemical reaction or in interactions with the substrate. These data suggest that one role of this conserved residue is to facilitate important *millisecond* protein dynamics.

During the performance of their biological functions, proteins necessarily change conformation. The time scales and amplitudes of these motions vary widely, yet these dynamics parameters are accessible by solution NMR spin-relaxation experiments, which generally encompass two time windows, the pico−nanosecond and micro−millisecond regimes. Changes in protein dynamics on the pico−nanosecond time scale can make measurable contributions to protein configurational entropy (*1*−*3*), which in turn can play an important energetic role in ligand binding (*4*−*8*). These changes in protein dynamics often occur at multiple amino acid sites throughout the protein structure. The pathway linking these flexible protein regions is believed to be selected by evolutionary forces, which optimize energetic coupling between functionally important residues (*9*−*11*). The network of these coupled residues provides for cooperativity between local processes occurring at the ligand-binding site and important global protein dynamics (*12*).

In addition to the fast protein dynamics described above, protein motions on a much slower time scale (micro−millisecond) can participate directly in many processes such as enzyme catalysis (*13*−*15*), rate-limiting conformational transitions (*16*−*20*), disulfide bond isomerization (*21*), protein folding (*22*−*24*), allosterism (*25*, *26*), and ligand−protein and protein−protein recognition (*27*−*30*). In many cases of ligand binding or catalysis, the micro−millisecond motions that occur are not limited to the active site or ligand-recognition site but are global in nature, similar to the aforementioned pico−nanosecond processes. Given the prime importance of these slow motions to protein function, it is also likely that the amino acid residues participating in these processes are conserved and subject to evolutionary pressures (*28*, *30*, *31*). However, little information is available regarding what changes in dynamics occur during function, how these conserved residues act in a global manner, or what effects the alteration of a particular amino acid has on dynamics and function.

The question of how a global dynamic process is coordinated and controlled throughout the protein structure is an essential one in biophysics. These conformational fluctuations of the enzyme structure are essential for catalytic function and in some cases are rate-limiting to the overall catalyzed reaction (*20*). We have previously demonstrated, using ribonuclease A (RNase A) as a model system, that it possesses an intrinsic global dynamic, which enables it to exist in equilibrium between the major, open (apo) conformation and a minor, closed (substrate-bound) conformation in the absence of the substrate (*17*). Similarly, when bound to the substrate, RNase A exists predominantly in the closed conformation yet still conformationally samples the open configuration to some extent, indicating that the enzyme has a built-in propensity to access the catalytically important configurations, regardless of the presence of the substrate (*17*). These conformational changes occur at a time scale identical to the rate-limiting enzymatic step (*16*), which is product-release. Thus, the rate-limiting step is controlled by the conformational change in this enzyme (*32*, *33*). This phenomenon of pre-existing equilibrium is the basis of the MWC model of cooperativity (*34*) and was suggested as operational in antibody-binding specificity (*35*). This notion was subsequently demonstrated in an enzyme system using pre-steady-state kinetics studies that revealed the existence of a conformational equilibrium between active and inactive states (*36*). Solution and solid-state NMR experiments have shown that this phenomenon, the innate ability of an enzyme to access catalytically important conformations, may be widespread (*37*, *38*). Particularly suited for NMR dynamics studies is RNase A, an enzyme in which protein-wide millisecond dynamics are known to be important for function

* To whom correspondence should be addressed. Telephone: 203-436-4847. Fax: 203-432-6144. E-mail: patrick.loria@yale.edu.

10.1021/bi0525066 CCC: $33.50
Published on Web 02/04/2006

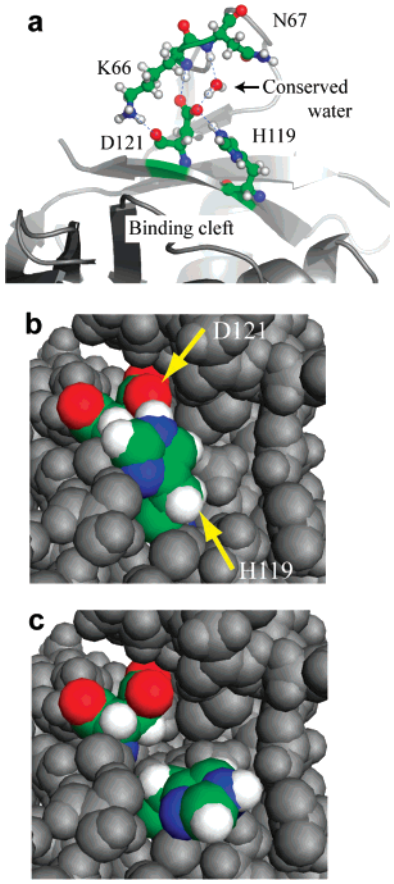

FIGURE 1: Structural environment of the D121−H119 catalytic dyad in RNase A. (a) Important active-site residues of RNase A are shown as a ball-and-stick model on a cartoon representation of RNase A (PDB entry 7RSA) (*42*). K66 and N67 are located in loop 4, and H119 and D121 are located in β sheet 6. A conserved water molecule hydrogen-bonded to D121 and N67 is shown as a ball-and-stick representation. (b and c) Two known conformations of the catalytic acid H119 are shown as observed in the crystal structure (*47*). D121 and H119 are represented by space-filling models. H119 assumes position A in b and position B in c.

(*16*, *17*, *32*, *33*, *39*, *40*). Here, we address the issue of the motional mechanism for *millisecond* time-scale events, their coordination, and their implications for function. These issues are investigated by solution NMR studies on RNase A at discrete steps along the enzyme reaction coordinate using three catalytically relevant complexes: the apo enzyme, the enzyme−substrate (ES), and the enzyme−product (EP) forms of the wild type (WT) and a site-directed mutant (D121A).

The conserved, acidic residue, D121, provides the main link between the active-site pocket (β sheet 6), where the phosphoester cleavage occurs, and loop 4, which contains the amino acid functional groups that endow RNase A with binding specificity for purine nucleotides located on the 5′ side of bond cleavage (Figure 1a). In the WT enzyme, this acidic residue is located near the active site but does not directly participate in catalysis (*41*). The principal, structural role of the carboxylate moiety of D121 is participation in a hydrogen bond that bridges the active site and the purine-binding site by linking the catalytically essential general acid, H119, a conserved water molecule, and K66/N67, which are located in the purine-binding loop (loop 4) (Figure 1a) (*42*). Aspartic acid 121 is absolutely invariant along with histidine 119 in known mammalian pancreatic, seminal, and brain ribonucleases, in eosinophil associated ribonucleases, and in angiogenin (*43*). The strict conservation of the D121/H119 pair has earned the name "catalytic dyad" based on the analogy of this pair within the serine protease family.

RNase A catalyzes the scission of a single-stranded RNA molecule and has a strong preference for cleavage between purines and pyrimidines (*44*, *45*). The substrate binds in a groove located between two halves of the enzyme, straddling the active site, with the purine portion binding on one side making contacts with loop 4 and the pyrimidine binding on the other. Catalysis occurs via a general acid/base process, in which the conserved residue, H12, increases the nucleophilicity of the 2′-ribose hydroxyl facilitating the attack of this 2′ oxygen on the adjacent 3′-phosphorus atom. The other catalytically essential histidine, H119, which protonates the leaving group 5″ oxygen, completes the reaction. The rate-limiting step occurs after chemistry and involves a global conformational change in the enzyme; the resulting catalytic rate occurs at $\sim$1600 s^{-1} at 298 K. In the WT RNase A enzyme the rate-determining product release step is linked to a conformational change that results in opening/closing of the cleft around the active site (*46*). These conformational changes are relatively modest but encompass distant elements of the RNase A structure (Figure 2). The largest of these changes are localized to loop regions. In particular, loop 4 at the active site (Figure 2b) moves closer to the substrate, as do loops 2 and 5. In addition, loop 1 at the base of the active-site cleft undergoes a conformational change in response to ligand binding (Figure 2).

Consistent with the observed structural changes, NMR dynamics experiments demonstrated that global conformational motion occurs at the same rate as k_{cat} and implicated this motion as being part of the rate-determining step (*16*, *17*), suggesting a link between protein dynamics and the slow step in the catalytic cycle of this enzyme. The mechanism whereby these conformational changes at the active site are coupled to the global conformational motion that facilitates product release is investigated here by the mutation of the conserved residue D121 to alanine. Importantly, D121 makes no direct interactions with the substrate or product. In the ES complex, the carboxyl side chain of D121 is >7 Å from the site of bond cleavage and 6.8 Å from the C2 ribose on the pyrimidine (*17*) (Figure 2b). Similarly, this side chain is 10 Å from O2 of the pyrimidine ribose and 6.8 Å from the nearest phosphoryl oxygen in the 3′-CMP product complex (EP) (*47*). This mutation, in addition has no significant effect on the enzyme structure based on X-ray crystallographic comparison of D121A and WT enzymes (*41*). Furthermore, detailed biochemical and biophysical studies have shown that the k_{cat}/K_m versus pH profiles for WT and D121A are indistinguishable (*41*) and the microscopic pK_a values of the two active-site histidines in D121A differ by $\sim$0.1 pH unit from the WT value (*48*). Thus, this mutation does not affect the chemical properties of the essential active-site acids/bases or the tertiary structure of the enzyme, yet the D121A mutant is 90% less active than the WT enzyme. We assessed whether severing the link between β sheet 6 and loop 4, by substitution of alanine at position 121, disrupts the global or local protein dynamics in RNase A or alters the rate-limiting product release (k_{off}) value. The kinetics of three important motional processes were characterized by solution NMR: (1) the product release rate, (2) the protein backbone conformational exchange rate, and (3) the dynamics of the

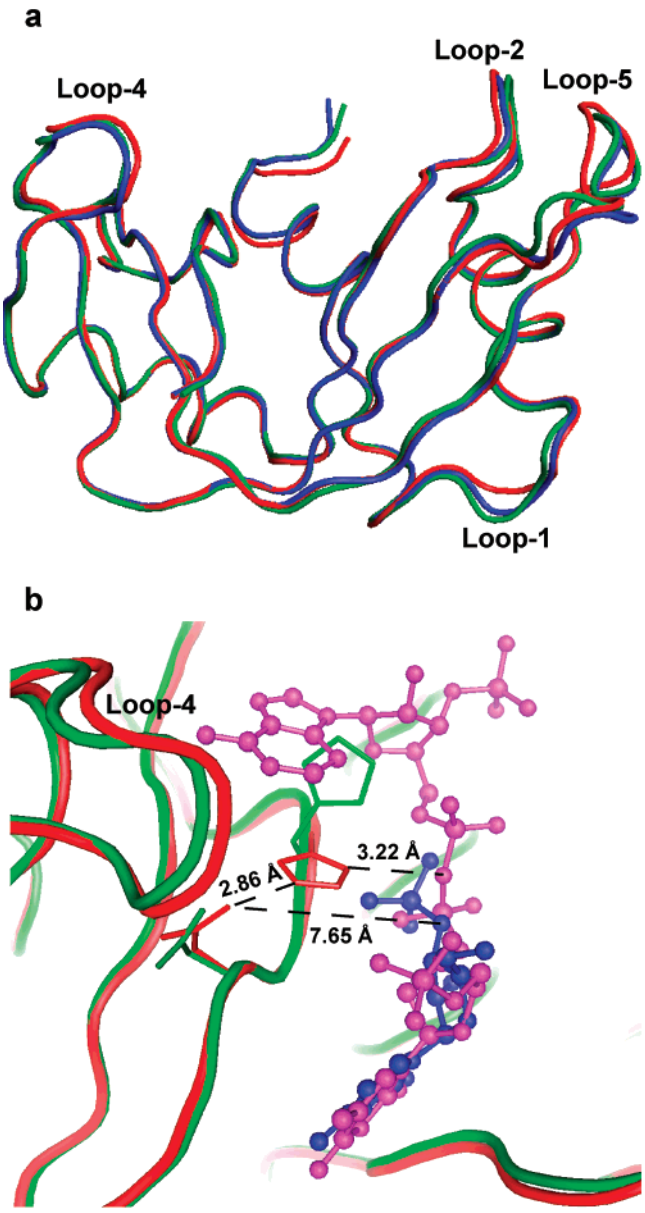

FIGURE 2: Three-dimensional structure of RNase A. (a) Overlay of three crystal structures of RNase A in the apo (blue), E−pTppAp (red), and E−3′CMP (green) complexes. Loop regions with the largest rmsd between the structures are labeled. (b) Close-up view of the active site for the ES and EP mimics, E−pTppAp (red), and E−3′CMP (green), respectively. The substrate analogue, pTppAp, is shown in magenta, and the product pyrimidine, 3′-CMP, is shown in blue. The side chains of D121 and H119 are shown with distances indicated by dashed lines to provide perspective. The crystal structures used are apo [7RSA (*42*)], pTppAp [1U1B (*17*)], and 3′-CMP [4RSD (*47*)].

side chain of the active-site residue, H119. Here, it is demonstrated that the mutation of D121 has a significant impact on all of these processes.

MATERIALS AND METHODS

Protein Expression and Purification. The D121A mutation in the RNase A gene was performed using the QuikChange Mutagenesis Kit (Stratagene). Preparation of ^{15}N- and ^{15}N-^{13}C-labeled samples of RNase A was performed according to published protocols (*16*). The purity of the final protein samples was determined to be >95% using sodium dodecyl sulfate−polyacrylamide gel electrophoresis and MALDI−TOF mass spectrometry. The concentration of RNase A was assayed spectrophotometrically using an extinction coefficient, $\epsilon_{278} = 9800\ M^{-1}\ cm^{-1}$. 3′-CMP was purchased from Sigma Chemical (St. Louis, MO) and used without further purification. The substrate analogue pTppAp was prepared and characterized as described (*17*, *49*). This substrate analogue binds to RNase A in the low nanomolar range, and its binding was determined by titration calorimetry as described previously (*6*).

NMR Experiments. All protein NMR experiments were performed on 450−700 μM samples of ^{15}N- and ^{15}N-^{13}C-labeled RNase A at 25 °C. The solutions were unbuffered and contained 10 mM NaCl and 1.5 mM NaN_3. The sample pH was adjusted to 6.35 with HCl and was checked prior to every experiment. NMR data was acquired on Varian Inova 500, 600, and 800 MHz instruments equipped with HCN probes. The NMR sample temperature was calibrated for each experiment with 100% methanol. Relaxation-compensated CPMG (rcCPMG) experiments were performed to measure spin-relaxation rates of ^{15}N of amide groups on ^{15}N-labeled protein and $^{13}C^{\epsilon 1}$ nuclei of histidine side chains using ^{15}N-^{13}C-labeled RNase A. All rcCPMG experiments were acquired in a single interleaved pseudo-four-dimensional experiment. Relaxation rate dispersion analysis was performed as previously described (*17*). To quantitate the contribution of micro−millisecond chemical-exchange motion, $R_2(1/\tau_{cp})$ was measured using the rcCPMG experiment performed as a function of interpulse delay, τ_{cp} (*50*). At all chemical-exchange time scales, the value of $R_2(1/\tau_{cp})$ is related to the microscopic exchange parameters by (*51*−*53*)

$$R_2(1/\tau_{cp}) = \frac{1}{2}\left(R_{2A}^0 + R_{2B}^0 + k_{ex} - \frac{1}{\tau_{cp}}\cosh^{-1}[D_+ \cosh(\eta_+) - D_- \cos(\eta_-)]\right) \quad (1)$$

$$D_\pm = \frac{1}{2}\left[\pm 1 + \frac{\Psi + 2\Delta\omega^2}{(\Psi^2 + \zeta^2)^{1/2}}\right] \quad (2)$$

$$\eta_\pm = \frac{\tau_{cp}}{\sqrt{2}}[\pm\Psi + (\Psi^2 + \zeta^2)^{1/2}]^{1/2} \quad (3)$$

$$\Psi = (R_{2A}^0 - R_{2B}^0 - p_A k_{ex} + p_B k_{ex})^2 - \Delta\omega^2 + 4p_A p_B k_{ex}^2 \quad (4)$$

$$\zeta = 2\Delta\omega(R_{2A}^0 - R_{2B}^0 - p_A k_{ex} + p_B k_{ex}) \quad (5)$$

in which p_A and p_B are the equilibrium populations of the two sites, $\Delta\omega$ is the difference in chemical shifts between the two sites, R_{2A}^0 and R_{2B}^0 are the intrinsic transverse relaxation rates in the absence of chemical exchange, and k_{ex} is the microscopic exchange rate constant of the motional process. The exchange rate constant k_{ex} for nuclei in equilibrium between two magnetically inequivalent sites (A ↔ B) is the sum of the rate constants for the forward and reverse processes. Determination of the microscopic rate constant by measuring R_2 as a function of the interpulse delay τ_{cp} is known as dispersion analysis.

Transverse spin-relaxation data using the rcCPMG experiment (*50*) for the apo, pTppAp, and 3′-CMP saturated

enzyme samples were acquired at 800, 600, and 500 MHz at 298 K. At each static magnetic field, $R_2(1/\tau_{cp})$ relaxation rates were measured by acquiring two-dimensional experiments with interpulse delays, τ_{cp} during the nitrogen relaxation period of 0.625, 0.714, 1.0, 1.25, 1.67, 2.0, 2.50, 3.33, 5.0, and 10.0 ms. Relaxation rates were determined from a reference experiment with a total relaxation time equal to 0.0 ms and one with the total relaxation time equal to 40.0 ms (*19*). The proton carrier frequency was set coincident with the water resonance. The ^{15}N carrier was set to 119 ppm. Dispersion data for each amino acid residue were analyzed using in-house fitting algorithms written in Mathematica code (Wolfram, Inc.), which utilizes the Levenberg−Marquardt algorithm (*54*). Determination of the sign of the chemical-shift difference between the exchanging conformations was performed as described by Kay and co-workers (*55*).

The kinetics of the 3′-CMP interaction with WT and D121A RNase A were measured by titration of 3′-CMP into a solution of ^{15}N-^{13}C-labeled enzyme. The ^{15}N-HSQC spectra were recorded at each titration point. Line-shape analysis was performed in MATLAB as described (*17*).

J-Coupling Constant Measurements. Measurements of ^3J-coupling constants between C′ and C$^\gamma$ and between ^{H}N and C$^\gamma$ of histidine residues were performed using 2D-triple resonance *J*-quantitative experiments (*56*) and analyzed to obtain χ_1 angles using a parametrized Karplus equation (*57*, *58*). The dependencies of the ^3J-coupling constants in a histidine side chain were calculated using the Fourier-series form equations and the amino-acid-specific Karplus coefficients (*57*, *58*)

$$^3J = C_0 + C_1 \cos\theta + C_2 \cos 2\theta \qquad (6)$$

in which the coefficients $\theta = \chi_1$ (degrees), $C_0 = 1.30$ Hz, $C_1 = -0.49$ Hz, and $C_2 = 0.65$ Hz for $^3J_{NC\gamma}$ and $\theta = \chi_1 - 120°$, $C_0 = 2.14$ Hz, $C_1 = -0.87$ Hz, and $C_2 = 1.15$ Hz for $^3J_{C'C\gamma}$. The delays allowing the evolution of the scalar coupling interactions ranged from 50 to 130 ms.

Dispersion Curve Simulations. A total of 1000 synthetic $R_2(\tau_{cp})$ data sets were generated for a two-site exchange process using exchange parameters, $k_{ex} = 1000$ s^{-1}, $\Delta\omega^{11.7\ T} = 950$ s^{-1} ($\Delta\omega^{18.8\ T} = 1500$ s^{-1}), $p_a = 0.95$, and $R_2^0 = 15$ s^{-1}. Each set was modified by incorporating random errors in the $R_2(\tau_{cp})$ values; errors were selected from a Gaussian distribution with full width at half-maximum at 5%. Each of the 1000 data sets included 12 error-incorporated $R_2(\tau_{cp})$ values, where τ_{cp} ranged between 714 μs and 65.0 ms ($\nu_{cpmg} = (1/\tau_{cp}) \sim [1400\ s^{-1} - 15\ s^{-1}]$) to reflect experimentally practical values for ^{15}N relaxation experiments on modern NMR spectrometers. To assess the quality of exchange parameters that can be expected from experimental data, we fit eq 1 to each of the 1000 synthetic $R_2(\tau_{cp})$ data sets. Nonlinear least-squares fits were executed using Prism 4.0 (GraphPad Software, Inc.) and were constrained so that (1) $0.8 \le p_a \le 1.0$ (i.e., $p_a \gg p_b$), (2) $R_2^0 > 10$ s^{-1}, (3) $k_{ex} > 100$ s^{-1}, and (4) $\Delta\omega > 50$ s^{-1} for two-site exchange. The R_2^0 constraint is reasonable for ^{15}N nuclei in a macromolecule the size of RNase A, while restrictions on p_a, k_{ex}, and $\Delta\omega$ limits these parameters to values observed previously for this enzyme.

RESULTS

Interactions of RNase A with Ligand. Steady-state NMR line-shape analysis (*17*) was performed on the WT enzyme during a titration with the product analogue, 3′-CMP, to quantitate the kinetics of the rate-limiting product release step. The chemical-shift changes for protein ^{1}H and ^{15}N resonances were quantitated from a series of 2D HSQC experiments with progressive increases in the 3′-CMP concentration (Figure 3a). A total of 26 residues shifted significantly in the WT enzyme upon binding to 3′-CMP; 15 of these were quantifiable (sufficiently resolved in all spectra). The dissociation constant for 3′-CMP is in the micromolar range and therefore could be quantitated from the changes in these NMR chemical-shift values. The resulting dissociation constant (K_d) for WT RNase A is 210 ± 30 μM (Figure 3a, black curve). There is very little variation in the dissociation constants determined by independent fits of the individual residue-specific changes in chemical shifts, indicating that all residues report on the same binding event; the values reported henceforth are those from a simultaneous fit for all residues to a single K_d value. For WT RNase A, NMR line-shape analysis of the 3′-CMP titration series yields a ligand-binding rate (k_{on}) = 8.1 ± 0.7 × 10^6 M^{-1} s^{-1} and dissociation rate constant (k_{off}) = 1700 ± 150 s^{-1} (Figure 3b).

As in the WT enzyme, several residues in the D121A variant experience chemical-shift changes in response to the interaction with 3′-CMP (of a total of 36, 13 were quantifiable). The residues experiencing chemical-shift perturbations by titration with 3′-CMP are the same in WT and D121A. The resulting dissociation constant for 3′-CMP from these titration experiments, determined by global fitting, is 78 ± 13 μM (Figure 3a, red curve), indicating that the product analogue binds with higher affinity to D121A than it does to the WT enzyme. However, the line-shape analysis (Figure 3b) of the 3′-CMP titration reveals that the increased affinity results from increases in both the k_{on} and k_{off} values. For D121A, $k_{on} = 3.5 \pm 0.2 \times 10^7$ M^{-1} s^{-1} and $k_{off} = 2700 \pm 150$ s^{-1}.

^{15}N Backbone Dynamics. The millisecond backbone amide dynamics of the WT enzyme were quantitated by measuring the rate of decay of ^{15}N transverse coherence, $R_2(\tau_{cp})$, as a function of ^{15}N-180° pulse-repetition time, τ_{cp} (Figure 4a) (*50*). In total, 29, 23, and 33 amino acid residues in the apo, ES, and EP complexes experience conformational exchange motion (Figure 5a). Statistical analysis (*17*) of the NMR data indicate that these regions of RNase A possess the same global conformational exchange rate, $k_{ex} = 1750 \pm 130$ s^{-1} in the apo form, in the ES complex, $k_{ex} = 1900 \pm 250$ s^{-1}, and in the EP form, $k_{ex} = 1730 \pm 75$ s^{-1} (parts c and d of Figure 5).

Typical relaxation dispersion curves for D121A are shown in parts b and c of Figure 4. Identical analysis of the backbone motion in D121A indicates that 34, 23, and 27 residues experience conformational exchange, respectively, in the apo, ES, and EP forms (Figure 5b). The identity of these flexible residues in D121A is essentially the same as those found for WT, except for residues in and near loop 4 (Figure 5b, cyan circle). In the apo and 3′-CMP forms of D121A, the global exchange rate is elevated relative to the WT enzyme with k_{ex} values of 2400 ± 70 and 2000 ± 80

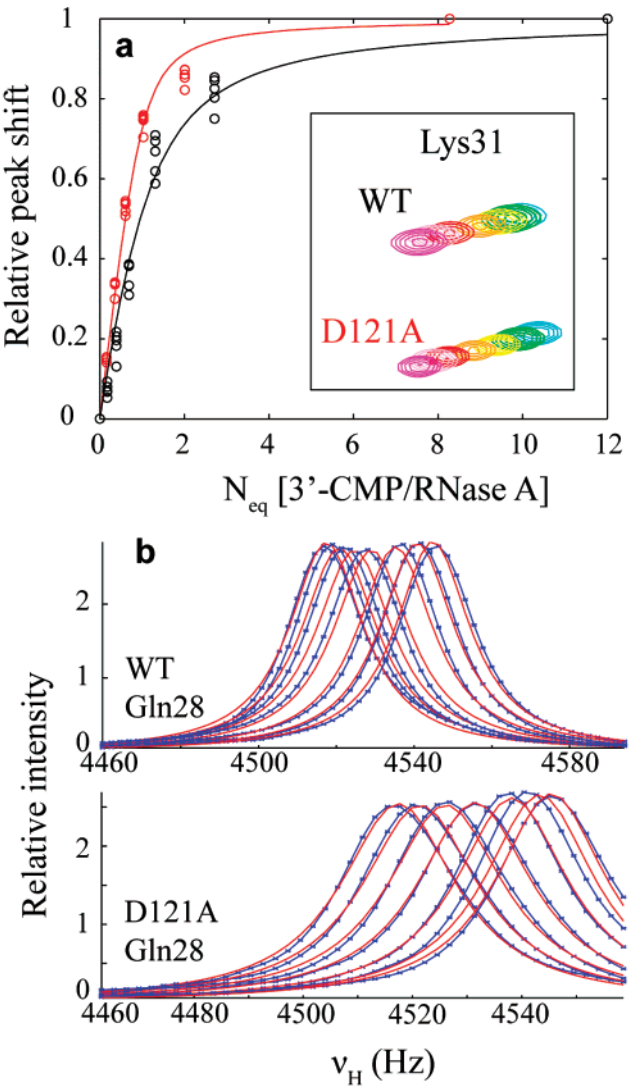

FIGURE 3: Binding kinetics of 3′-CMP to the WT and D121A RNase A. Results of a titration series and NMR line-shape analysis. (a and the inset) Titration of the product, 3′-CMP, is followed by monitoring the changes in backbone chemical shifts observed in ^{1}H-^{15}N HSQC spectra for WT (black) and D121A (red) RNase A. The analysis was performed on a set of residues assigned and resolved in spectra of both D121A and WT enzymes, His12, Met13, Gln28, Lys31, and Thr36. Circles correspond to normalized, experimentally measured changes in chemical shifts for this group of residues and were used for global fitting, with solid lines representing the fitted curve. The inset to a shows, as an example, the changes in chemical shifts for Lys31 in WT (top) and D121A (bottom) RNase A upon an increase in the 3′-CMP concentration. The contour plots, going from left to right, correspond to the number of equivalents of 3′-CMP/WT RNase A, 0, 0.174, 0.393, 0.691, 1.31, 2.71, and 12; and 3′-CMP/D121A RNase A, 0, 0.159, 0.354, 0.602, 1.03, 2.01, and 8.27. The fits yield $K_d = 210 \pm 30$ μM for WT RNase A and $K_d = 78 \pm 13$ μM for D121A RNase A. (b) Results of NMR line-shape fitting for Gln28 for WT and D121A RNase A. Blue symbols and connecting lines correspond to experimental NMR data, and red solid curves represent the global, multiresidue line-shape fitting curves. For WT RNase A, nonlinear fitting gives $k_{off} = 1700 \pm 150$ s^{-1}, and for D121A RNase A, nonlinear fitting gives $k_{off} = 2700 \pm 150$ s^{-1}.

s^{-1}, respectively. In addition, unlike the dynamics observed in WT RNase A, the purine-binding loop 4 shows no evidence of millisecond dynamics (compare Asn71, in parts a and b of Figure 4) except for C65. Thus, many of the residues (K66, N71, and C72) in the vicinity of loop 4 lose WT-like flexibility, whereas the remainder of the enzyme experiences a slightly increased exchange rate in the mutant. Removal of the interaction between β sheet 6 and loop 4 by mutation of D121 disrupts the WT-like motion in the enzyme. Furthermore, in the ES complex, the relaxation dispersion data are no longer best described by a single, global rate constant (parts c and e of Figure 5). The relaxation dispersion data for the ES complex were best modeled with two separate dynamics processes in which residues were partitioned into a fast- and a slow-exchanging group as indicated in Figure 5c (right graph). Residues in the fast group were S15, S16, T17, A19, S22, S80, and Q101, whereas residues in the slow group consisted of T3, A5, Q11, N27, M29, M30, S32, N34, L35, C40, A64, C65, R85, G112, H119, and A121. Fitting of each group of residues with eq 1 gave k_{ex} values and populations (p_a) of 2380 $\pm$ 300 s^{-1}, 94 $\pm$ 2% and 730 $\pm$ 70 s^{-1}, 85 $\pm$ 8% for the fast and slow groups, respectively. Statistical F tests (*59*) and AIC (*60*) analysis demonstrates that the "two-k_{ex} model" is a much better descriptor of the relaxation data in the D121A ES complex than a model with a single, global k_{ex} value. In comparison to the two models, the F ratio is 155, giving a p value < 0.0001. Likewise, the difference in AIC values for the two models is 250. The spatial location and partitioning of the fast- and slow-exchanging residues is depicted in Figure 5e. In the case of the WT and D121A enzymes, fractional populations for the major conformer range between 85 and 94%, but 5% uncertainties in these values preclude interpretation.

To make meaningful interpretations of the exchange rate constants, k_{ex}, obtained from relaxation dispersion experiments, an accurate assessment of the exchange parameters (k_{ex}, p_a, $\Delta\omega$, and R_2^0), given a set of experimental data, is needed (*61*). To estimate the faithfulness of the experimentally determined exchange parameters, 1000 synthetic data sets were generated for a two-site exchange model with relaxation data at two static magnetic fields using exchange conditions similar to those expected for RNase A. The distribution of fit parameters is shown in Figure 6. These results show that, assuming 5% uncertainty in the data, simultaneous fitting to the relaxation data at two magnetic fields accurately reproduces the input parameters. Thus, the experimental data in this study can be reliably interpreted.

Histidine Side-Chain Conformations. To more fully characterize the aspects of the mutation of D121 on the active site, two sets of ^{3}J couplings were measured for histidine side chains. The active-site acid, H119, in the WT enzyme is known to undergo a rotation about its C_α−C_β bond to interconvert between the trans and gauche$^+$ ($\chi_1 = 159°/\chi_1 = -60°$) conformers; the resulting conformations are called A and B, respectively (parts b and c of Figure 1). For the apo-WT enzyme, the measured $^{3}J_{C'C\gamma} \leq 2.3$ Hz ($^{3}J_{NC\gamma}$ was not measurable because of spectral overlap), and for apo-D121A, the upper limit of $^{3}J_{C'C\gamma} = 2.5$ Hz and the value of $^{3}J_{NC\gamma} = 1.6 \pm 0.1$ Hz (Figure 7). These three-bond coupling constants report on the χ_1 angle and are consistent with allowed values for H119 that are a time average between trans and gauche$^+$ conformations. Gauche$^-$ conformations are rarely seen in proteins (*62*) and would additionally require major backbone conformational changes to occur in RNase A. Therefore, the D121A variant enzyme retains the WT-

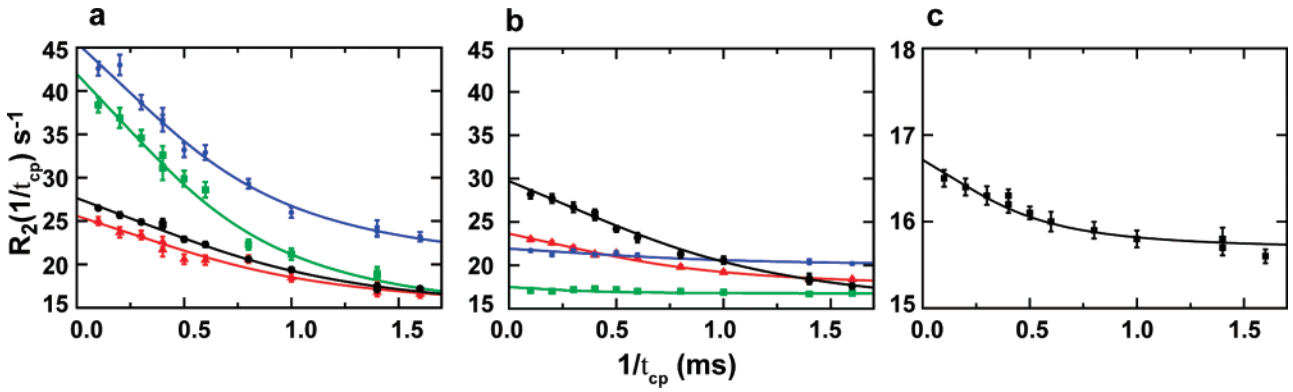

FIGURE 4: Differences in millisecond dynamics observed in WT and D121A RNase A. (a, b, and c) Dispersion curves (at 800 MHz) obtained for WT (a) and D121A (b) RNase A characterizing amide ^{15}N conformational exchange for residues S16 (black), S80 (red), N71 (green) and H119 (blue). (c) Dispersion profile for C65 in D121A RNase A. The data shown was obtained at 800 MHz, but the curves represent the global fit utilizing spin-relaxation data at both 800 and 600 MHz.

like character in which H119 interconverts between conformations A and B. For H12, χ_1 for both the mutant and WT are also the same (not shown).

Histidine Side-Chain Dynamics. Because the conformation of H119 has important implications on the function of RNase A, its motion was investigated by NMR relaxation studies. To achieve this, we have developed an NMR experiment to probe relaxation at the $C^{\epsilon 1}$ position of histidine residues to allow for characterization of the dynamics of the imidazole ring (see the Supporting Information). Simultaneous fitting of $C^{\epsilon 1}$ spin-relaxation data at two magnetic fields (11.7 and 18.8 T) indicates that the side chain of H119 in apo-WT RNase A moves at a rate, $k_{ex} = 1670 \pm 130$ s^{-1} (Figure 8a), which is the same as the backbone dynamics rate and the ligand dissociation rate (*vide supra*). In contrast, for the D121A apo enzyme, the $C^{\epsilon 1}$ NMR relaxation experiments show that the H119 imidazole ring experiences conformational motion on a time scale $\sim 3000-5000$ s^{-1} (Figure 8b). For motional dynamics of this rate, nonlinear fitting to relaxation-compensated CPMG data is not reliable, and therefore, we are able to determine a limited range for H119 side-chain motion. These spin-relaxation data indicate that the conformational exchange rate constant for the side chain of H119 is also at least 2-fold greater than that seen in the WT enzyme.

In studies of conformationally mobile systems such as this, typically, one observes a single population-weighted chemical shift, which is positioned intermediate between the chemical shifts of the invisible, interchanging conformations. The difference between these invisible resonances is given by $\Delta\omega$ and is obtained from fits of the rcCPMG spin-relaxation data. The value of $\Delta\omega$ obtained from this analysis can be augmented with information of its sign ($\pm$), which provides the locations of chemical shifts for the major and minor conformations involved in the exchange process. The sign and magnitude of $\Delta\omega$ for residues in loop 1 in the mutant and WT complexes of RNase A are provided in Figure 9. For these residues, which are distant from the active site, the signs of $\Delta\omega$ for the bound forms are opposite that for the apo enzymes. This is the case for both the WT and D121A enzymes. In addition, the magnitude of $\Delta\omega$ is similar when comparing the same ligated forms of WT and D121A, suggesting similar conformations for loop 1 in both mutant and WT enzymes at each position on the reaction coordinate.

DISCUSSION

The mechanism of how global protein dynamics are coordinated and perhaps impact on enzyme catalytic rates is an important one if a thorough understanding of the protein function is to be obtained. It has been suggested that important dynamics are subject to evolutionary pressures in much the same way as a protein fold or function evolves (*63*). Computational and experimental work has provided support for this notion in dihydrofolate reductase in which pico−nanosecond motions of conserved residues were demonstrated to have a substantial impact on hydride transfer (*64*, *65*). Here, we investigated the role of a conserved residue in *millisecond* dynamics by a comparison of mutant and WT enzymes at discrete stages along the enzymatic reaction coordinate. This mutation of a conserved residue, by all measures, does not affect the structure of RNase A or the chemical properties of the active site yet is disruptive to the catalytic turnover rate. In addition, the pico−nanosecond (see the Supporting Information) and microsecond dynamics (not shown) of the RNase A backbone are unaffected by this mutation. However, this mutation causes significant effects on the *millisecond* dynamics of this enzyme.

Given the role of conformational changes in gating the rate-limiting product release step (*32*), the interaction of the product, 3′-CMP, with D121A and WT was determined by NMR line-shape analysis. For the WT enzyme, the measured dissociation rate constant for 3′-CMP is identical to the k_{cat} value, as expected for an enzyme in which this step is rate-limiting. For D121A, the k_{off} value is elevated by 1000 s^{-1} relative to the WT value (Table 1). The on rate for 3′-CMP binding to D121A is also elevated in comparison to the WT, resulting in a higher affinity of 3′-CMP for D121A. Although D121 does not interact directly with the ligand, it nevertheless plays a role in defining the kinetics of ligand/protein interactions. Because protein dynamics in RNase A are important for the rate-determining step (*32*), we further investigated the *millisecond* motions in the E, ES, and EP complexes of RNase A via ^{15}N-amide backbone relaxation dispersion experiments.

Parts a and b of Figure 5 show the location of the flexible sites in RNase A in the E, ES, and EP complexes. The location of the flexible residue is very similar in all three enzyme forms (*17*). In the WT, these sites all move with the same global rate constant (Table 1), and this rate constant

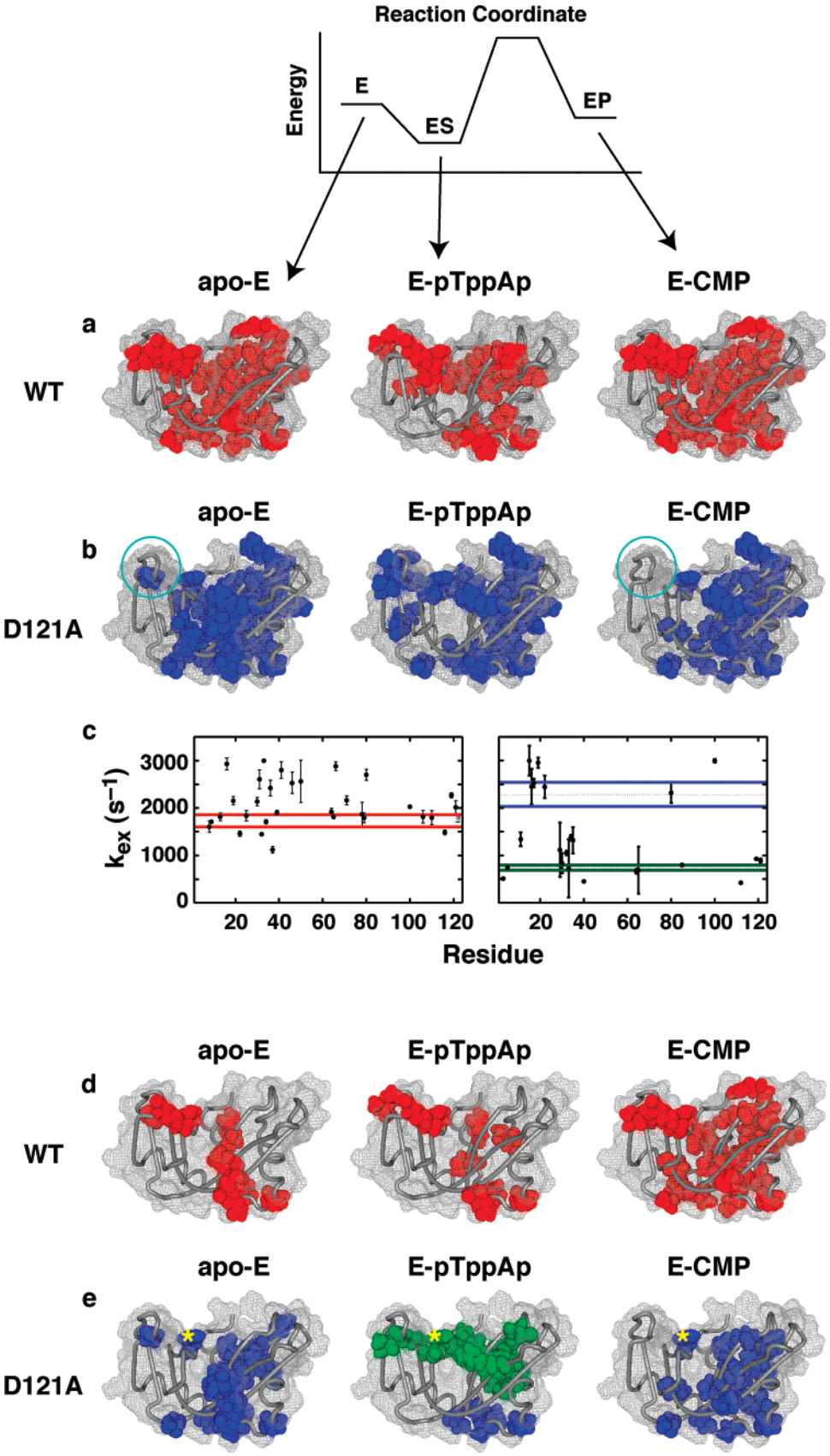

FIGURE 5: Spatial location of conformationally mobile residues in RNase A. Residues that show an increase in $R_2(1/\tau_{cp})$ with increasing τ_{cp} values are mapped onto the ribbon structure of RNase A for (a) WT and (b) D121A for the E, ES, and EP complexes going from left to right, respectively, and shown diagrammatically with the reaction coordinate located at the top of the graph. (c) Individually fit k_{ex} values (●) for residues in WT (left) and D121A (right) in the RNase A/pTppAp complex. The solid, colored lines indicate the 95% confidence interval for the global fitted k_{ex} value for all residues in WT and for residues in D121A with $k_{ex} > 1500$ s^{-1} (blue) and $k_{ex} < 1500$ s^{-1} (green). (d and e) Subset of quantifiable k_{ex} values for all enzyme complexes are mapped onto the ribbon structure of RNase A using the same color scheme as in c. The location of the D121 mutation is indicated with a gold asterisk in e, and loop 4 is circled in b.

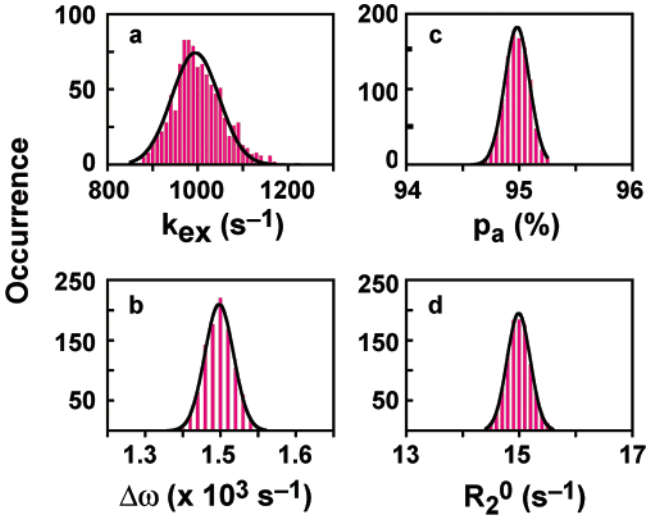

FIGURE 6: Parameter distribution (two magnetic fields). Histogram of the parameter estimates for (a) k_{ex}, (b) $\Delta\omega$, (c) p_a, and (d) R_2^0 from fitting eq 1 to 1000 synthetic data sets simultaneously at 11.7 and 18.8 T magnetic fields. Input parameters were $k_{ex} = 1000\ s^{-1}$, $\Delta\omega^{11.7\ T} = 950\ s^{-1}$ ($\Delta\omega^{18.8\ T} = 1500\ s^{-1}$), $p_a = 0.95$, $R_2^0 = 15\ s^{-1}$. The resulting distributions are modeled with a single Gaussians.

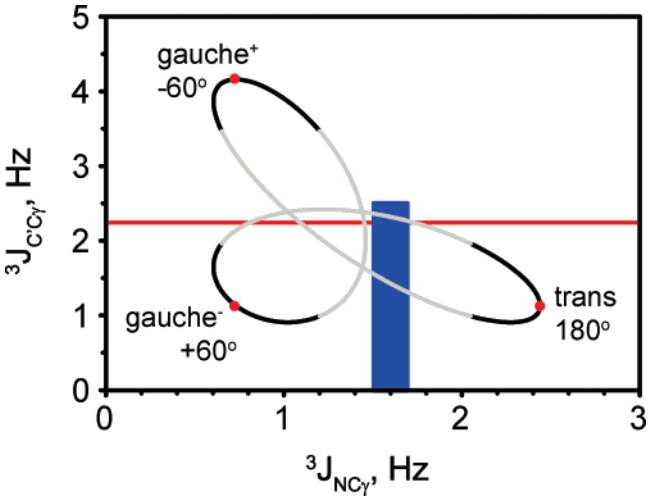

FIGURE 7: Parametric plot of ^3J-coupling constants. The parametric form of the dependence of the ^3J-coupling constants on the torsion angle χ_1 allows for easier identification of the torsion-angle ranges, satisfying experimentally measured values of *both* $^3J_{C'C\gamma}$- and $^3J_{NC\gamma}$-coupling constants. The plot corresponds to the values of the histidine torsion angle χ_1 ranging from $-180°$ to $+180°$. Major rotameric states are labeled and shown as red dots. The gray line corresponds to the eclipsed conformations ($\pm 30°$). The red line corresponds to the experimental upper limit of $^3J_{C'C\gamma}$ in WT H119. The blue-shaded area is defined by experimentally measured values of both $^3J_{NC\gamma}$ and $^3J_{C'C\gamma}$ in H119 for D121A.

is the same in each enzyme complex and as noted previously the same as the catalytic rate (*16*). These and additional data discussed below suggest that the backbone conformation of the WT enzyme exists in two conformations and that binding of ligand, whether the substrate or product, affects the relative populations of these conformations but not the kinetics of the conformational interconversion. In the mutant enzyme, the flexible sites are essentially the same as in the WT enzyme with the exception of loop 4. In contrast to the WT enzyme, there are differences in the kinetics of the backbone dynamics of D121A in the E and EP complexes. With the exception of C65, the dynamics in loop 4 are no longer

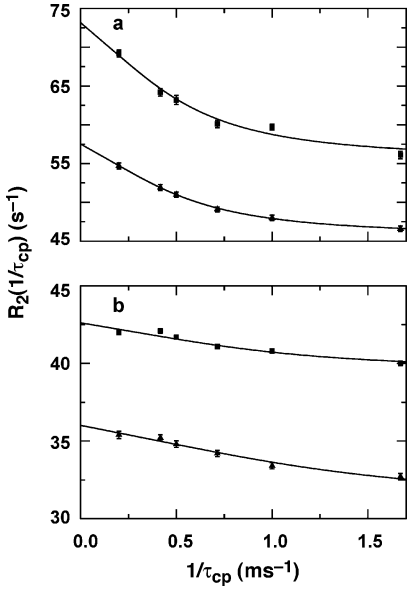

FIGURE 8: Histidine side-chain dynamics. Histidine $C^{\epsilon 1}$ dispersion curves for (a) WT and (b) D121A enzymes. Relaxation rates for the $C^{\epsilon 1}$ position of H119 at 500 (▲) and 800 (■) MHz as a function of the 180° ^{13}C pulse repetition rate. Curves are a simultaneous fit to the data at both static magnetic field strengths.

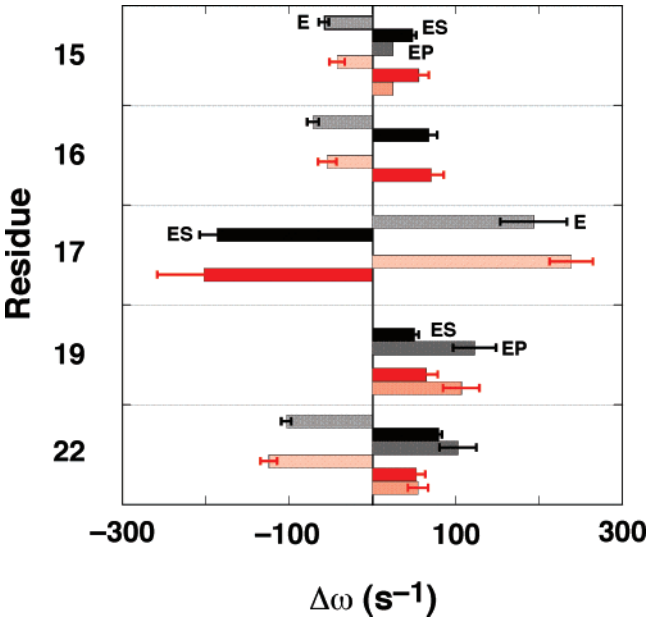

FIGURE 9: Magnitude and sign of chemical-shift differences. The magnitude of the chemical-shift difference was determined by fitting eq 1 to the NMR spin-relaxation data for residues in loop 1 for the WT (black) and D121A (red) forms of RNase A. The magnitude is plotted for the apo-E (hatched), E−pTppAp (solid), and E−CMP (stippled) forms of the enzyme. The sign of $\Delta\omega$ was determined from a pair of HSQC/HMQC ^1H-^{15}N spectra as described previously (*55*). For enzyme complexes in which no error bars are shown on the data bar, only the sign of $\Delta\omega$ could be determined; the magnitude is given an arbitrary value of 25 s^{-1} for graphical purposes only.

detectable (Figure 5b, left and right panels, cyan circle). This suggests that removing the D121 interaction uncouples the global dynamic process. It is possible that the apparent loss of dynamics in this loop could be due to $\Delta\omega \cong 0$, caused by the removal of the carboxylate group in residue 121. However, we have also investigated the dynamics of the D121N mutant and observe similar results as in D121A,

Table 1: Summary of Rate Constants for WT and D121A RNase A

type of motion	WT (s^{-1})	D121A (s^{-1})
backbone dynamics (apo RNase A)	1750 ± 130	2400 ± 70[a]
backbone dynamics (RNase A/pTppAp)	1900 ± 250	2400 ± 300[b] 730 ± 70[c]
backbone dynamics (RNase/CMP)	1730 ± 75	2000 ± 80[a]
product release rate	1700 ± 150	2700 ± 150
H119 $C^{\epsilon 1}$ dynamics	1670 ± 130	3000−5000
k_{cat}	1600	60

[a] Experiences global motion with the exception of residues in loop 4 in which the motion was not detectable. [b] Motional rate for loop 1 only. [c] Motional rate for active-site region and loop 4.

suggesting that the effect is not simply due to the changes in the chemical environment in this region (not shown).

The dynamics of WT loop 4 did not simply shift to another time scale in D121A because both the WT and mutant display identical order parameters (see the Supporting Information) and identical microsecond motions obtained from off-resonance $R_1\rho$ experiments (not shown). In addition to the absence of a detectable motion in loop 4, the exchange rate k_{ex} for the conformational motion, for residues outside of this loop, in each of these mutant enzyme complexes is elevated relative to the WT. These differences are not large (1700−1900 s^{-1} for the WT versus 2000−2400 s^{-1} for D121A), but they are real and reproducible. Interestingly, the backbone dynamics in the mutant and WT are similar to their respective product release rates as determined by lineshape analysis. Thus, even in the mutant, protein dynamics appear to modulate ligand release, although the impaired catalytic turnover rate in D121A indicates that this step is not rate-limiting as it is in the WT enzyme.

In the D121A ES complex, the changes in dynamics are striking. Unlike the WT enzyme, in which the ES complex experiences a global dynamics process, the dynamics of D121A−pTppAp could not be adequately described by a single rate constant (parts c and e of Figure 5). The residues in loop 1 move with an exchange rate of $2400 \pm 300 s^{-1}$, whereas the remainder of the flexible residues, which comprise the active site and loop 4, move at a much slower rate of 730 ± 70 s^{-1}. This conformational change is the result of intramolecular motion and is not due to pTppAp binding/dissociation because the excess amount of ligand ensures an insignificant population of free enzyme (*17*). In this mutant enzyme, the kinetics of the active-site motion in the ES complex are damped relative to the WT enzyme. In addition, loop 4 in the D121A−pTppAp complex shows evidence of conformational motion unlike the apo and 3′-CMP-bound forms of this mutant enzyme. Thus, it appears that the ligand, which bridges the active site and loop 4, aids in transmitting the global motion from the enzyme to this loop yet not with the same efficiency of D121. 3′-CMP, which does not bridge the purine and pyrimidine sites, is unable to elicit motion in loop 4 like that of the substrate analogue pTppAp. Unlike in the WT enzyme, ligand binding in D121A alters the kinetics of the conformational exchange process with the additional separation of motion into two time scales in the ES complex.

The effects of mutation on the dynamics of the active site, in particular that of the side chain of H119, were investigated with a new solution NMR experiment designed to measure *millisecond* dynamics in histidine side chains. Using this experiment, the motion of H119 in the WT was determined to be identical to all other dynamic processes in the enzyme, whereas in D121A, the imidazole ring of H119 moves at a significantly elevated rate. Here, we assume that the motion detected by NMR $C^{\epsilon 1}$ dispersion experiments is the trans/gauche$^+$ (A/B) interconversion observed in X-ray crystal (*66*) and solution NMR (*67*) studies of RNase A. Our ^3J-coupling measurements confirmed that conformational averaging similar to the one seen in the WT is present in D121A RNase A (Figure 7). In conformation A, $N^{\delta 1}$ of H119 is properly positioned to protonate the leaving group of 5′ oxygen of the substrate. After protonation, H119 must be reprotonated prior to a subsequent catalytic cycle. In conformer B, $N^{\delta 1}$ is not correctly positioned to perform its acidic function but rather is hydrogen-bonded to a water molecule (*41*), from which it is able to be reprotonated. Thus, the motion of H119 bears on the RNA cleavage reaction because it must be in position A for catalysis to occur. These NMR spin-relaxation data indicate that this dynamic process is altered upon the mutation of the conserved residue D121.

In protein dynamics studies, it is important to not only address the kinetics of the conformational motion but also the magnitude of this motion. Insight into enzyme motion can be obtained from consideration of $\Delta\omega$ (*21*) and its direction (*55*). We have previously used this type of analysis to provide evidence that conformational changes in apo and substrate-mimicked WT RNase A represent an example of a ligand-stabilized conformational change (*17*) in a manner analogous to the MWC model of allosterism (*34*). Here, we extend this analysis to the EP complex and to the D121A mutant enzyme. The results are depicted in Figure 9. These residues shown in Figure 9 are located in loop 1, approximately 25 Å from the active-site histidine residues. Loop 1 alters its conformation depending upon the ligation state of RNase A (Figure 2a). Motion of this loop is part of a structural change involving α helix 2 and β sheets 1 and 4. These changes allow active-site residues in RNase A to make intimate contact with the substrate or product. Conversion between these two conformations in the WT enzyme is part of the global conformational change, which determines the rate of product release. As such, the dynamics of this loop as well the active-site and substrate-binding loop 4 occur at a rate matched to the catalytic turnover value. The position of loop 1 correlates well with the conformation of the purine-binding loop (loop 4). This correlation is also observed in normal-mode analysis of RNase A (not shown). These data indicate that the conformation of loop 1 is a particularly useful gauge of the conformational state of RNase A. Importantly, the residues in loop 1 are distant from the active site, and therefore, differences in chemical shifts observed for these residues should report only on conformational changes and should not be complicated by additional electrostatic effects because of the proximity to the charged ligand in the bound enzyme. For WT RNase A, the data in Figure 9 show that the values of $\Delta\omega$ for the liganded (ES and EP) forms of RNase A are of similar magnitude to each other and to the apo enzyme but of opposite sign to the apo enzyme. This observation supports, as we described previously for the WT-pTppAp form, the notion that RNase A is

in equilibrium between open/closed conformations, in which ligand binding shifts the relative populations to the bound (closed) form in this pre-existing dynamic process (*17*).

An identical analysis of the sign and magnitude of $\Delta\omega$ for D121A indicates that a similar equilibrium is at play in this mutant form, further supporting a likely two-state equilibrium between bound and free enzyme conformations. The similarity of the magnitude of $\Delta\omega$ values for each residue in loop 1 and the identical sign of $\Delta\omega$ for these residues in D121A and WT in the apo, ES, and EP complexes further suggest that the conformational changes in D121A and WT are similar if not the same; the result of this mutation disrupts the kinetics of the exchange process but not its magnitude.

These experiments demonstrate that D121 provides a link that allows for the coupling of motion involved in global protein dynamics. In the WT, H119 motion, the protein backbone dynamics, and the release of ligand all occur with the same rate constant (Table 1); in D121A, these rates are elevated and span a range of values from 2000 to 5000 s^{-1} with the additional complexity that loop 4 loses much of the conformational exchange behavior that it experiences in the WT enzyme. Moreover, the global dynamics observed in the WT ES complex do not exist in the substrate-bound form of D121A. This suggests that a principal role of the conserved residue, D121, is to help transmit and coordinate the dynamics of the active site with other important regions in the enzyme. The identical time scale of all of these dynamic processes (Table 1) underscores the global, coordinated dynamic that exists in WT RNase A.

For WT RNase A, the identity of all of the measured rate constants (Table 1) demonstrates the exquisite synchrony of dynamics in this enzyme. The mutation of D121 to alanine clearly disrupts the timing of these motions. In this mutant, k_{cat} decreases from the WT value of 1600 to 60 s^{-1}. Although it seems unlikely that this mutation would have introduced a slower dynamic process that is responsible for the decreased catalytic rate, we nonetheless have performed ^{15}N *zz*-exchange experiments (*68*−*70*) to look for such a process occurring at ∼60 s^{-1}. These experiments have not detected evidence for such slow motion. The question remains, *if and how* disruption of WT dynamics influences the catalytic rate. One possible scenario would be that disruption of dynamics from concerted (WT) to a more stepwise[1] process (D121A) could lead to a decrease in the overall rate for catalytic turnover. Thus, disruption of concerted dynamics could possibly account for some of the rate deceleration observed in the mutant enzyme. Furthermore, the disruption of the H119 side-chain motion could alter the population (*41*) of its catalytically important conformation, resulting in additional detrimental effects on catalysis, although more work is needed to fully identify the mechanism. Nonetheless, this study exemplifies the importance of protein dynamics in enzyme function and suggests that the inconcinnity in dynamics imparted by the mutation of D121 is likely a reason for its strict conservation.

[1] Here, "stepwise" is used to indicate that the dynamics processes are no longer synchronized and not to suggest that the mutation induces some specific order in the dynamic events.

ACKNOWLEDGMENT

J. P. L. acknowledges support from NSF-CAREER award (MCB-0236966) and the Alfred P. Sloan Foundation.

SUPPORTING INFORMATION AVAILABLE

Description of experimental procedures used for the histidine-specific relaxation measurements; Figure S1, free histidine $^{13}C_{\epsilon 1}$ dynamics measurements; and Figure S2, similarity in N−H order parameters for WT and D121A RNase A. This material is available free of charge via the Internet at http://pubs.acs.org.

REFERENCES

1. Yang, D., and Kay, L. E. (1996) Contributions to conformational entropy arising from bond vector fluctuations measured from NMR-derived order parameters: Application to protein folding, *J. Mol. Biol. 263*, 369−382.
2. Li, Z., Raychaudhuri, S., and Wand, A. J. (1996) Insights into the local residual entropy of proteins provided by NMR relaxation, *Protein Sci. 5*, 2647−2650.
3. Akke, M., Brüschweiler, R., and Palmer, A. G. (1993) NMR order parameters and free energy: An analytic approach and application to cooperative Ca^{2+} binding by calbindin D_{9k}, *J. Am. Chem. Soc. 115*, 9832−9833.
4. Stivers, J. T., Abeygunawardana, C., and Mildvan, A. S. (1996) ^{15}N NMR relaxation studies of free and inhibitor-bound 4-oxalocrotonate tautomerase: Backbone dynamics and entropy changes of an enzyme upon inhibitor binding, *Biochemistry 35*, 16036−16047.
5. Zidek, L., Novotny, M. V., and Stone, M. J. (1999) Increased protein backbone conformational entropy upon hydrophobic ligand binding, *Nat. Struct. Biol. 6*, 1118−1121.
6. Kovrigin, E. L., Cole, R., and Loria, J. P. (2003) Temperature dependence of the backbone dynamics of ribonuclease A in the ground state and bound to the inhibitor 5′-phosphothymidine (3′−5′) pyrophosphate adenosine 3′-phosphate, *Biochemistry 42*, 5279−5291.
7. Bracken, C., Carr, P. A., Cavanagh, J., and Palmer, A. G. (1999) Temperature dependence of intramolecular dynamics of the basic leucine zipper of GCN4: Implications for the entropy of association with DNA, *J. Mol. Biol. 285*, 2133−2146.
8. Lee, A. L., Kinnear, S. A., and Wand, A. J. (2000) Redistribution and loss of side chain entropy upon formation of a calmodulin−peptide complex, *Nat. Struct. Biol. 7*, 72−77.
9. Lockless, S. W., and Ranganathan, R. (1999) Evolutionarily conserved pathways of energetic connectivity in protein families, *Science 286*, 295−299.
10. Suel, G. M., Lockless, S. W., Wall, M. A., and Ranganathan, R. (2003) Evolutionarily conserved networks of residues mediate allosteric communication in proteins, *Nat. Struct. Biol. 10*, 59−69.
11. Wand, A. J. (2001) Dynamic activation of protein function: A view emerging from NMR spectrscopy, *Nat. Struct. Biol. 8*, 926−931.
12. Fuentes, E. J., Der, C. J., and Lee, A. L. (2004) Ligand-dependent dynamics and intramolecular signaling in a PDZ domain, *J. Mol. Biol. 335*, 1105−1115.
13. Eisenmesser, E. Z., Bosco, D. A., Akke, M., and Kern, D. (2002) Enzyme dynamics during catalysis, *Science 295*, 1520−1523.
14. Osborne, M. J., Schnell, J., Benkovic, S. J., Dyson, H. J., and Wright, P. E. (2001) Backbone dynamics in dihydrofolate reductase complexes: Role of loop flexibility in the catalytic mechanism, *Biochemistry 40*, 9846−9859.
15. Venkitakrishnan, R. P., Zaborowski, E., McElheny, D., Benkovic, S. J., Dyson, H. J., and Wright, P. E. (2004) Conformational changes in the active site loops of dihydrofolate reductase during the catalytic cycle, *Biochemistry 43*, 16046−16055.
16. Cole, R., and Loria, J. P. (2002) Evidence for flexibility in the function of ribonuclease A, *Biochemistry 41*, 6072−6081.
17. Beach, H., Cole, R., Gill, M., and Loria, J. P. (2005) Conservation of μs−ms enzyme motions in the apo- and substrate-mimicked state, *J. Am. Chem. Soc. 127*, 9167−9176.

18. Evenas, J., Malmendal, A., and Akke, M. (2001) Dynamics of the transition between open and closed conformations in a calmodulin C-terminal domain mutant, *Structure 9*, 185−195.
19. Mulder, F. A., Skrynnikov, N. R., Hon, B., Dahlquist, F. W., and Kay, L. E. (2001) Measurement of slow (μs−ms) time scale dynamics in protein side chains by ^{15}N relaxation dispersion NMR spectroscopy: Application to Asn and Gln residues in a cavity mutant of T4 lysozyme, *J. Am. Chem. Soc. 123*, 967−975.
20. Codreanu, S. G., Ladner, J. E., Xiao, G. Y., Stourman, N. V., Hachey, D. L., Gilliland, G. L., and Armstrong, R. N. (2002) Local protein dynamics and catalysis: Detection of segmental motion associated with rate-limiting product release by a glutathione transferase, *Biochemistry 41*, 15161−15172.
21. Grey, M. J., Wang, C., and Palmer, A. G., III (2003) Disulfide bond isomerization in basic pancreatic trypsin inhibitor: Multisite chemical exchange quantified by CPMG relaxation dispersion and chemical shift modeling, *J. Am. Chem. Soc. 125*, 14324−14335.
22. Korzhnev, D. M., Salvatella, X., Vendruscolo, M., Di Nardo, A. A., Davidson, A. R., Dobson, C. M., and Kay, L. E. (2004) Low-populated folding intermediates of Fyn SH3 characterized by relaxation dispersion NMR, *Nature 430*, 586−590.
23. Tollinger, M., Skrynnikov, N. R., Mulder, F. A., Forman-Kay, J. D., and Kay, L. E. (2001) Slow dynamics in folded and unfolded states of an SH3 domain, *J. Am. Chem. Soc. 123*, 11341−11352.
24. Hill, R. B., Bracken, C., DeGrado, W. F., and Palmer, A. G. (2000) Molecular motions and protein folding: Characterization of the backbone dynamics and folding equilibrium of α D-2 using C-13 NMR spin relaxation, *J. Am. Chem. Soc. 122*, 11610−11619.
25. McElroy, C., Manfredo, A., Wendt, A., Gollnick, P., and Foster, M. (2002) TROSY−NMR studies of the 91 kDa TRAP protein reveal allosteric control of a gene regulatory protein by ligand-altered flexibility, *J. Mol. Biol. 323*, 463−473.
26. Stevens, S. Y., Sanker, S., Kent, C., and Zuiderweg, E. R. (2001) Delineation of the allosteric mechanism of a cytidylyltransferase exhibiting negative cooperativity, *Nat. Struct. Biol. 8*, 947−952.
27. Feher, V. A., and Cavanagh, J. (1999) Millisecond-time-scale motions contribute to the function of the bacterial response regulator protein Spo0F, *Nature 400*, 289−293.
28. McKercher, S. R., Lombardo, C. R., Bobkov, A., Jia, X., and Assa-Munt, N. (2003) Identification of a PU.1−IRF4 protein interaction surface predicted by chemical exchange line broadening, *Proc. Natl. Acad. Sci. U.S.A. 100*, 511−516.
29. Ding, Z., Lee, G., Liang, X., Gallazzi, F., Arunima, A., and van Doren, S. R. (2005) PhosphoThr peptide binding globally rigidifies much of the FHA domain from arabidopsis receptor kinase-associated protein phosphatase, *Biochemistry 44*, 10119−10134.
30. Mittermaier, A., Varani, L., Muhandiram, D. R., Kay, L. E., and Varani, G. (1999) Changes in side-chain and backbone dynamics identify determinants of specificity in RNA recognition by human U1A protein, *J. Mol. Biol. 294*, 967−979.
31. Li, Y.-C., and Montelione, G. T. (1995) Human type-α transforming growth factor undergoes slow conformational exchange between multiple backbone conformations as characterized by nitrogen-15 relaxation measurements, *Biochemistry 34*, 2408−2423.
32. Cathou, R. E., and Hammes, G. G. (1965) Relaxation spectra of ribonuclease. I. The interaction of ribonuclease with cytidine 3′-phosphate, *J. Am. Chem. Soc. 86*, 3240−3245.
33. Hammes, G. G. (2002) Multiple conformational changes in enzyme catalysis, *Biochemistry 41*, 8221−8228.
34. Monod, J., Wyman, J., and Changeux, J.-P. (1965) On the nature of allosteric transitions: A plausible model, *J. Mol. Biol. 12*, 88−118.
35. Pauling, L. (1940) A theory of the structure and process of formation of antibodies, *J. Am. Chem. Soc. 62*, 2643−2657.
36. Fersht, A. R., and Requena, Y. (1971) Equilibrium and rate constants for the interconversion of two conformations of chymotrypsin. The existence of a catalytically inactive conformation at neutral pH, *J. Mol. Biol. 60*, 279−290.
37. Eisenmesser, E. Z., Millet, O., Labeikovsky, W., Korzhnev, D. M., Wolf-Watz, M., Bosco, D. A., Skalicky, J. J., Kay, L. E., and Kern, D. (2005) Intrinsic dynamics of an enzyme underlies catalysis, *Nature 438*, 117−121.
38. Williams, J. C., and McDermott, A. E. (1995) Dynamics of the flexible loop of triosephosphate isomerase: The loop motion is not ligand gated, *Biochemistry 34*, 8309−8319.
39. Cathou, R. E., and Hammes, G. G. (1965) Relaxation spectra of ribonuclease. III. Further investigation of the interaction of ribonuclease and cytidine 3′-phosphate, *J. Am. Chem. Soc. 87*, 4674−4680.
40. Rasmussen, B. F., Stock, A. M., Ringe, D., and Petsko, G. A. (1992) Crystalline ribonuclease A loses function below the dynamical transition at 220 K, *Nature 357*, 423−424.
41. Schultz, L. W., Quirk, D. J., and Raines, R. T. (1998) His···Asp catalytic dyad of ribonuclease A: Structure and function of the wild-type, D121N, and D121A enzymes, *Biochemistry 37*, 8886−8898.
42. Wlodawer, A., Svensson, L. A., Sjolin, L., and Gilliland, G. L. (1988) Structure of phosphate-free ribonuclease A refined at 1.26 Å, *Biochemistry 27*, 2705−2717.
43. Altschul, S. F., Gish, W., Miller, W., Myers, E. W., and Lipman, D. J. (1990) Basic local alignment search tool, *J. Mol. Biol. 215*, 403−410.
44. McPherson, A., Brayer, G., Cascio, D., and Williams, R. (1986) The mechanism of binding of a polynucleotide chain to pancreatic ribonuclease, *Science 232*, 765−768.
45. Katoh, H., Yoshinaga, M., Yanagita, T., Ohgi, K., Irie, M., Beintema, J. J., and Meinsma, D. (1986) Kinetic studies on turtle pancreatic ribonuclease-A comparative study of the base specificities of the B2 and P0 sites of bovine pancreatic ribonuclease-A and turtle pancreatic ribonuclease, *Biochim. Biophys. Acta 873*, 367−371.
46. Hammes, G. G. (1982) *Enzyme Catalysis and Regulation*, Academic Press, New York.
47. Zegers, I., Maes, D., Dao-Thi, M. H., Poortmans, F., Palmer, R., and Wyns, L. (1994) The structures of RNase A complexed with 3′-CMP and d(CpA): Active site conformation and conserved water molecules, *Protein Sci. 3*, 2322−2339.
48. Quirk, D. J., and Raines, R. T. (1999) His···Asp catalytic dyad of ribonuclease A: Histidine pK_a values in the wild-type, D121N, and D121A enzymes, *Biophys. J. 76*, 1571−1579.
49. Leonidas, D. D., Shapiro, R., Irons, L. I., Russo, N., and Acharya, K. R. (1999) Toward rational design of ribonuclease inhibitors: High-resolution crystal structure of a ribonuclease A complex with a potent 3′,5′-pyrophosphate-linked dinucleotide inhibitor, *Biochemistry 38*, 10287−10297.
50. Loria, J. P., Rance, M., and Palmer, A. G. (1999) A Relaxation-compensated Carr−Purcell−Meiboom−Gill sequence for characterizing chemical exchange by NMR spectroscopy, *J. Am. Chem. Soc. 121*, 2331−2332.
51. Carver, J. P., and Richards, R. E. (1972) A general two-site solution for the chemical exchange produced dependence of T_2 upon the Carr−Purcell pulse separation, *J. Magn. Res. 6*, 89−105.
52. Davis, D. G., Perlman, M. E., and London, R. E. (1994) Direct measurements of the dissociation-rate constant for inhibitor−enzyme complexes via the $T_{1\rho}$ and T_2 (CPMG) methods, *J. Magn. Reson., Ser. B 104*, 266−275.
53. Jen, J. (1978) Chemical exchange and NMR T_2 relaxation−The multisite case, *J. Magn. Reson. 30*, 111−128.
54. Marquardt, D. W. (1963) *J. Soc. Ind. App. Math. 11*, 431−441.
55. Skrynnikov, N. R., Dahlquist, F. W., and Kay, L. E. (2002) Reconstructing NMR spectra of "invisible" excited protein states using HSQC and HMQC experiments, *J. Am. Chem. Soc. 124*, 12352−12360.
56. Hu, J.-S., Grzesiek, S., and Bax, A. (1997) Two-dimensional NMR methods for determining χ_1 angles of aromatic residues in proteins from three-bond $J_{C'C\gamma}$ and $J_{NC\gamma}$ couplings, *J. Am. Chem. Soc. 119*, 1803−1804.
57. Schmidt, J. M., Blumel, M., Lohr, F., and Ruterjans, H. (1999) Self-consistent ^3J-coupling analysis for the joint calibration of Karplus coefficients and evaluation of torsion angles, *J. Biomol. NMR 14*, 1−12.
58. Perez, C., Lohr, F., Ruterjans, H., and Schmidt, J. M. (2001) Self-consistent Karplus parametrization of ^3J couplings depending on the polypeptide side-chain torsion χ_1, *J. Am. Chem. Soc. 123*, 7081−7093.
59. Devore, J. (2000) *Probability and Statistics for Engineering and the Sciences*, Brooks/Cole Publishing Company, Monterey, CA.
60. Akaike, H. (1973) in *Proceedings of the 2nd International Symposium on Information Theory* (Petrov, B. N., and Csaki, F., Eds.) pp 267−281, Budapest, Hungary.
61. Kovrigin, E. L., Kempf, J. G., Grey, M., and Loria, J. P. (2005) Faithful estimation of dynamics parameters from relaxation dispersion measurements, *J. Magn. Reson.*, in press.

62. Kleywegt, G. J., and Jones, T. A. (1998) Databases in protein crystallography, *Acta Crystallogr., Sect. D: Biol. Crystallogr. 54*, 1119−1131.
63. James, L. C., and Tawfik, D. S. (2003) Conformational diversity and protein evolution−A 60-year-old hypothesis revisited, *Trends Biochem. Sci. 28*, 361−368.
64. Agarwal, P. K., Billeter, S. R., Rajagopalan, P. T., Benkovic, S. J., and Hammes-Schiffer, S. (2002) Network of coupled promoting motions in enzyme catalysis, *Proc. Natl. Acad. Sci. U.S.A. 99*, 2794−2799.
65. Cameron, C. E., and Benkovic, S. J. (1997) Evidence for a functional role of the dynamics of glycine-121 of *Escherichia coli* dihydrofolate reductase obtained from kinetic analysis of a site-directed mutant, *Biochemistry 36*, 15792−15800.
66. Borkakoti, N., Moss, D. S., and Palmer, R. A. (1982) Ribonuclease-A. Least-sqares refinement of the structure at 1.45 Å resolution, *Acta Crystallogr., Sect. B: Struct. Sci. 38*, 2210.
67. Santoro, J., Gonzalez, C., Bruix, M., Neira, J. L., Nieto, J. L., Herranz, J., and Rico, M. (1993) High-resolution three-dimensional structure of ribonuclease A in solution by nuclear magnetic resonance spectroscopy, *J. Mol. Biol. 229*, 722−734.
68. Montelione, G. T., and Wagner, G. (1989) 2D chemical exchange NMR spectroscopy by proton-detected heteronuclear correlation, *J. Am. Chem. Soc. 111*, 3096−3098.
69. Wider, G., Neri, D., and Wuthrich, K. (1991) Studies of slow conformational equilibria in macromolecules by exchange of heteronuclear longitudinal 2-spin-order in a 2D difference correlation experiment, *J. Biomol. NMR 1*, 93−98.
70. Farrow, N., Zhang, O., Forman-Kay, J. D., and Kay, L. E. (1994) A heteronuclear correlation experiment for simultaneous determination of ^{15}N longitudinal decay and chemical exchange rates of systems in slow equilibrium, *J. Biomol. NMR 4*, 727−734.

BI0525066